A PRIORI ASSESSMENT AND MODELING OF COMPRESSIBILITY EFFECTS IN THE SOLENOIDAL DISSIPATION RATE EQUATION

Johannes Kreuzinger, Rainer Friedrich
Fachgebiet Strömungsmechanik
Technische Universität München
D-85747 Garching, Germany
johannes@flm.mw.tu-muenchen.de

Thomas B. Gatski
Computational AeroSciences Branch
NASA Langley Research Center
Hampton, Virginia 23681-2199, USA
t.b.gatski@larc.nasa.gov

ABSTRACT

Several attempts have been made in the literature to improve the ability of statistical models to predict turbulent compressible flows. As yet, it is not possible to accurately predict both free and wall-bounded flows with the same model under a variety of conditions. One drawback in these attempts has been the lack of sufficiently reliable data with which to assess the various terms arising in the turbulent transport equations. In this study, the exact terms of the solenoidal dissipation rate equation are calculated for the first time in both a compressible channel flow and a turbulent mixing layer. This data is then used to assess both the exact and modeled form of this equation. In its exact form, explicit compressibility terms appear. In addition, the terms that also appear in the incompressible equation now may vary differently under increased compressibility conditions. This latter effect can be either an indirect one, that is compressibility modifies mean quantities and Reynolds stresses, or a direct one, that is the processes in the solenoidal dissipation rate equation are themselves modified by compressibility. In order to separate the indirect and direct effects, it is assumed that the processes in the solenoidal dissipation rate equation are properly described by the available incompressible functional forms. The model coefficients are then determined by *a priori* tests. The direct effects appear if the coefficients depend on compressibility, and these effects have to be modeled additionally.

EXACT AND MODELED FORM OF THE SOLENOIDAL DISSIPATION RATE EQUATION

It has been shown (e.g. Sinha and Candler, 2003) that the solenoidal dissipation rate ε can be well approximated by the form $\varepsilon = \bar{\nu}\overline{\omega_i'\omega_i'}$, where $\overline{\omega_i'\omega_i'}$ is twice the enstrophy. Although its transport equation has been given previously, it is written here for completeness and in order to contrast some details with previous studies:

$$\frac{D\varepsilon}{Dt} = P_\varepsilon^1 + P_\varepsilon^2 + P_\varepsilon^3 + P_\varepsilon^4 + T_\varepsilon + D_\varepsilon - \Upsilon + F_\varepsilon + T_\varepsilon^c + B_\varepsilon + \frac{\varepsilon}{\bar{\nu}}\frac{D\bar{\nu}}{Dt} \ , \tag{1}$$

where

$$P_\varepsilon^1 = -2\bar{\nu}\overline{(u_{i,j}' - u_{j,i}')u_{k,j}'}\,\bar{u}_{i,k} \tag{2a}$$

$$P_\varepsilon^2 = -2\bar{\nu}\overline{(u_{i,j}' - u_{j,i}')u_{i,k}'}\,\bar{u}_{k,j} \ , \tag{2b}$$

are the turbulent production of dissipation due to mean rate of strain,

$$P_\varepsilon^3 = -2\bar{\nu}\overline{(u_{i,j}' - u_{j,i}')u_k'}\,\bar{u}_{i,jk} = -2\bar{\nu}\overline{\omega_i'u_k'}\,\bar{\omega}_{i,k} \tag{2c}$$

is the production due to the mean vorticity gradient,

$$P_\varepsilon^4 = -2\bar{\nu}\overline{(u_{i,j}' - u_{j,i}')u_{i,k}'u_{k,j}'} \tag{2d}$$

$$-\Upsilon = -2\bar{\nu}\overline{\left((u_{i,j}' - u_{j,i}')/\rho\right)_{,k}\tau_{ik,j}} \tag{2e}$$

are the net destruction of dissipation, and

$$T_\varepsilon = -\bar{\nu}\left(\overline{u_k'(u_{i,j}' - u_{j,i}')u_{i,j}'}\right)_{,k} \tag{2f}$$

$$D_\varepsilon = 2\bar{\nu}\left(\overline{(u_{i,j}' - u_{j,i}')\frac{1}{\rho}\tau_{ik,j}}\right)_{,k} \tag{2g}$$

are the turbulent transport and viscous diffusion. The remaining terms constitute the explicit compressibility contributions. These include

$$T_\varepsilon^c = \bar{\nu}\overline{(u_{i,j}' - u_{j,i}')u_{i,j}'u_{k,k}'} \tag{2h}$$

which is the compressible turbulent transport,

$$B_\varepsilon = 2\bar{\nu}\overline{(u_{i,j}' - u_{j,i}')\rho_{,j}p_{,i}/\rho^2} \tag{2i}$$

and

$$F_\varepsilon = -2\bar{\nu}\overline{(u_{i,j}' - u_{j,i}')\rho_{,j}\tau_{ik,k}/\rho^2} \tag{2j}$$

which are the contributions due to the component of the force on a volume element that is normal to the density gradient. The baroclinic term B_ε is due to the force exerted by the pressure gradient, F_ε is due to the force resulting from the viscous stress gradient. The last term on the RHS of Eq. (1) requires no modeling and is simply the variation of the mean

kinematic viscosity. In the cases to be examined here, this term can be neglected.

It should be noted that the partitioning used here contrasts with that used by Sinha and Candler (2003). Their partitioning of terms originating from the viscous term in the momentum equation differs from the one used here. They obtained a viscous diffusion term, $\mathrm{D}_\varepsilon^{S\&C}$, a viscous dissipation term, $\mathrm{Y}_\varepsilon^{S\&C}$, and a viscosity variation term, $\mathrm{C}_\varepsilon^{S\&C}$, that can be written as

$$\mathrm{D}_\varepsilon^{S\&C} = \bar{\nu}^2 \left(\overline{u'_{i,j}u'_{i,j} - u'_{i,j}u'_{j,i}}\right)_{,kk} \quad (3a)$$

$$-\mathrm{Y}_\varepsilon^{S\&C} = -2\bar{\nu}^2\overline{(u'_{i,j} - u'_{j,i})_{,k}u'_{i,jk}} \quad (3b)$$

$$\mathrm{C}_\varepsilon^{S\&C} = -\Upsilon + D_\varepsilon + F_\varepsilon + \frac{\varepsilon}{\bar{\nu}}\frac{D\bar{\nu}}{Dt} - \mathrm{D}_\varepsilon^{S\&C} + \mathrm{Y}_\varepsilon^{S\&C}. \quad (3c)$$

$\mathrm{Y}_\varepsilon^{S\&C}$ and $\mathrm{D}_\varepsilon^{S\&C}$ are the terms that appear in the case of incompressible flow with no property variation, and all effects of compressibility and property variation are contained in $\mathrm{C}_\varepsilon^{S\&C}$. This makes the term $\mathrm{C}_\varepsilon^{S\&C}$ difficult to interpret. For example, in supersonic channel flow at $M = 3.1$ (see Table I Case K6000n), C_ε and D_ε are in balance at the wall, and each have high values that reach three times the maximum of the destruction Υ. The terms used in the present study are well behaved even in regions of high viscosity gradients. In the limit of incompressible flow, with no mean property variations both formulations are equivalent, that is $F_\varepsilon \to 0$, $\mathrm{C}_\varepsilon^{S\&C} \to 0$, $\Upsilon \to \mathrm{Y}_\varepsilon^{S\&C}$ and $D_\varepsilon \to \mathrm{D}_\varepsilon^{S\&C}$.

Models are needed to close the production, destruction and transport terms in Eq. (1). These are given by:

$$P_\varepsilon^1 + P_\varepsilon^2 = -C_\varepsilon^1 \frac{\varepsilon}{K}\widetilde{u''_i u''_j}\tilde{U}_{i,j} \quad (4)$$

$$P_\varepsilon^4 - \Upsilon = -C_\varepsilon^2 \varepsilon^2/K \quad (5)$$

$$P_\varepsilon^3 = -C_1^3 \cdot \bar{\nu} C_\mu \frac{K^2}{\varepsilon}\tilde{U}^2_{i,kk} - C_2^3 \cdot \bar{\nu}\frac{K}{\bar{\rho}\varepsilon}(\bar{\rho}K)_{,m}\tilde{U}_{i,m}\tilde{U}_{i,kk} \quad (6)$$

$$T_\varepsilon = f_t \cdot \left[\frac{C_\mu}{\sigma_\varepsilon}\frac{\bar{\rho}K^2}{\varepsilon}(\bar{\rho}\varepsilon)_{,i}\right]_{,i} / \bar{\rho}^2 \ , \quad (7)$$

where C_μ is defined by $-\widetilde{u''_i u''_j} = C_\mu(K^2/\varepsilon)\tilde{U}_{i,j}$. The models for Eqs. (4) and (5) were originally proposed by Hanjalić and Launder (1972), and the model for P_ε^3 was developed by Rodi and Mansour (1993). The turbulent transport T_ε is modeled by a gradient diffusion model with $\sigma_\varepsilon = 1.3$. All these models were designed for incompressible flow and are adapted here for compressible flow by introducing variable density and viscosity, and Favre mean and fluctuation quantities. In the partitioning used here, the viscous diffusion term D_ε is not closed and it also has to be modeled.

The above models are used for *a priori* tests. From the DNS simulations, each quantity in the above equations is known, and the model coefficients C_ε^1, C_ε^2, C_1^3, C_2^3, f_t and C_μ can be determined. These coefficients can be calculated, and compressibility effects altering these quantities can be identified. The cases of channel flow and mixing layer will be studied separately. This will isolate the effects of compressibility in wall bounded and free shear flows.

All the direct simulations are performed using a finite-difference scheme for the primitive variables pressure, velocity and entropy. Integration in time is done by a third order Runge-Kutta scheme. Two different spatial discretizations are used: A fifth order compact upwind scheme in the case of channel flows, and an optimized fourth order central compact scheme plus filtering of the highest wavenumbers to stabilize the simulations in the case of the mixing layer.

Flow Case	$M = \frac{u_{av}}{c_w}$	$Re_{av} = \frac{\rho_{av} u_{av} H}{\mu_{av}}$
KM03	0.350	2808.6
K3000	1.5327	2452.2
K6000n	3.1399	3204.0

Table 1: Parameters of the DNS of channel flow with cooled walls. H is the channel half width, the subscript av denotes values averaged over the whole flow domain, w wall values.

COMPRESSIBILITY EFFECTS AND THEIR MODELING

In order to properly compare terms and model coefficients for the various Mach and Reynolds numbers, suitable scaling parameters have to be found. For the turbulent channel flow data analyzed here, Foysi *et al.* (2004) have successfully used $u_\tau^* = \sqrt{\tau_w/\bar{\rho}}$ as a fluctuating velocity scale, and $\bar{\mu}/\tau_w$ and H/u_{av} (u_{av} = volume averaged mean velocity) as the proper time scales for the near-wall and the core regions, respectively. This allows for the scaling of all the terms in the ε-equation which can then be plotted against the semi-local viscous coordinate $z^* = z\bar{\rho}u_\tau^*/\bar{\mu}$ close to the wall, and against z/H in the core region. In the mixing layer, one scaling is sufficient throughout the flow, namely Δu (velocity difference across the layer) for the velocity fluctuations, and $\delta_\theta/\Delta u$ for the timescale (δ_θ = momentum thickness). The relevant coordinate there is the self-similar coordinate $\zeta = z/\delta_\theta$.

CHANNEL FLOW

Channel flow simulations carried out by Foysi *et al.* (2004) are used here. The three channel flows (see Table 1) cover a substantial range of Mach numbers. The Reynolds number, defined from mean quantities, Re_{av} varies little between cases.

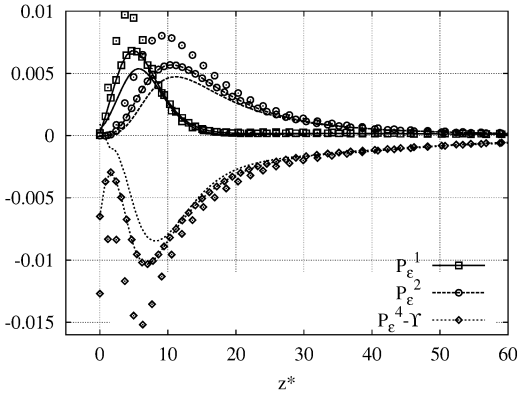

Figure 1: Production and destruction terms in the ε-equation; KM03 (symbols), K3000 (lines & symbols) and K6000n (lines)

The main effect of increasing Mach number is to increase the mean property variation in the range $z^* < 30$. This region is characterized by steep gradients of density and viscosity close to the cooled wall. For the three Mach number cases simulated, the wall density is 0.02, 0.37 and 1.54 times higher than the mean density. This effect is proportional to M^2. In

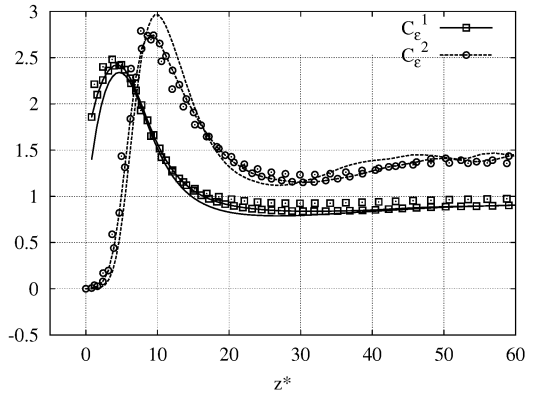

Figure 2: Model coefficient C_ε^1 and C_ε^2 variation across channel; KM03 (symbols), K3000 (lines & symbols) and K6000n (lines)

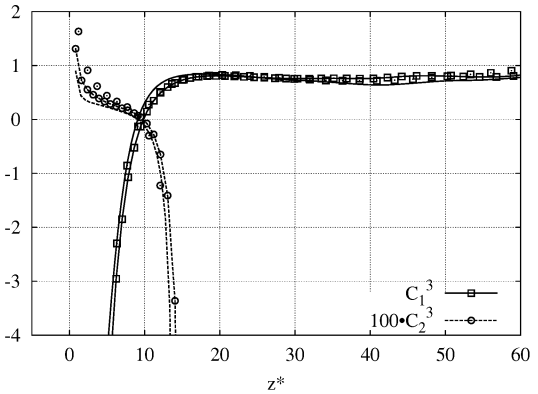

Figure 3: Model coefficient C_1^3 and C_2^3 variation across channel; KM03 (symbols), K3000 (lines & symbols) and K6000n (lines)

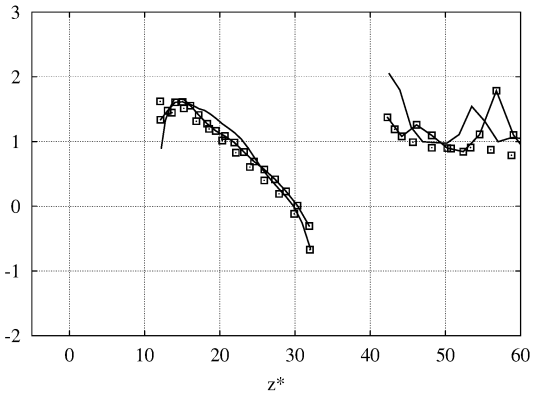

Figure 4: Model coefficient f_t variation across channel; KM03 (symbols), K3000 (lines & symbols) and K6000n (lines)

addition, any differences in mean velocity between the different cases are accounted for using the channel flow velocity scalings.

The near-wall scaling collapses the positions of the peaks of terms in the ε-equation (1), but the amplitudes show a monotonic decrease with increasing Mach number (Fig. 1). Only the explicit compressibility terms T_ε^c, B_ε and F_ε increase with Mach number, but they still remain negligible. At the wall the viscous diffusion D_ε decreases with increasing Mach

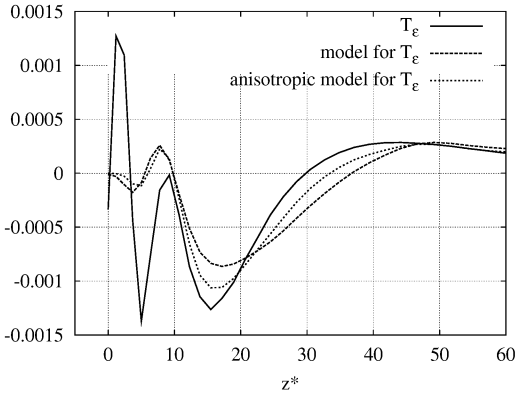

Figure 5: (—): T_ε; (– –): model Eq.(7), $f_t = 1.0$; (- - -) : $0.18 \cdot \left[\bar{\rho}\widetilde{u_i''u_j''}\frac{K}{\varepsilon}(\bar{\rho}\varepsilon)_{,j}\right]_{,i}/\bar{\rho}^2$; KM03

number. For $z^* > 30$ no compressibility effect was seen. This was also checked using an outer scaling for the center region of the channel.

Plotted in inner variables, the profiles of the coefficients C_ε^1 and C_ε^2 for the different Mach numbers collapse (see Fig. 2). This indicates that no compressibility effects influence either the production or destruction terms.

Unfortunately, evaluations of the models for P_ε^3 and T_ε are more difficult to interpret since these terms change sign across the channel. Some progress can be made, however, by examining each term of the model separately (see Eq. (6)). Figure 3 shows that the second term is only important near the wall ($z^* < 12$). This is exemplified by the relatively constant values of both C_1^3 and C_2^3 (≈ 0.7 and 0.007, respectively) in their respective regions of importance. C_1^3 shows no dependence on Mach number, C_2^3 is decreasing, but only slightly.

For the transport T_ε, there is a relatively good collapse of the data for the model coefficient f_t in the regions shown in Fig. 4. In the near-wall region ($z^* < 12$) and in the region $32 < z^* < 42$ (not shown), T_ε changes sign, so no meaningful value of the coefficient can be obtained. If directly compared to the exact term, the model works well except for a small region in close proximity to the wall (Fig. 5). An improvement of the model is possible, if the dependence on turbulent kinetic energy is replaced by individual Reynolds stress components.

In incompressible flows, the viscous diffusion term D_ε is modeled as $(\nu\varepsilon_{,i})_{,i}$. The incompressible model can be adapted to a compressible one directly by introducing a variable density and viscosity. This leads to $D_\varepsilon \approx (\bar{\mu}(\bar{\rho}\varepsilon)_{,i})_{,i}/\bar{\rho}^2$. A more general and more complex expression can be obtained from $D_\varepsilon \approx \partial^2\varepsilon^*/\partial z^{*2}$ which gives $D_\varepsilon \approx [\bar{\mu}(\bar{\rho}\varepsilon\bar{\mu})_{,i}/\sqrt{\bar{\rho}}]_{,i}\ /(\bar{\mu}\bar{\rho}^{\frac{3}{2}})$. The second formulation gives better results especially for high Mach numbers; although the behavior directly at the wall ($z^* < 3$) still cannot be captured exactly (not shown).

MIXING LAYER

The parameter range covered by the mixing layer simulation data is given in Table 2. From this database, it is possible to investigate the effect of different Mach numbers (M10 and M11) and mean property variation (M10 and M14). The mean density difference in simulation M14 is the same as in the channel flow simulation at $M = 3.1$, K6000n, and Re_θ is the average Reynolds number over the time interval that was used to average the data using self-similar normalization.

flow case	$M_c = \frac{\Delta U}{c_1+c_2}$	ρ_2/ρ_1	$Re_\theta = \frac{\rho_{av}\Delta U \delta_\theta}{\mu_{av}}$
M10	0.15	1	1072
M11	1.1	1	984
M14	0.197	2.7	941

Table 2: Parameters of the DNS of time dependent mixing layers. The subscripts 1 and 2 denote the lower and the upper stream, δ_θ the momentum thickness.

The box size and initial conditions are chosen as in the simulations described by Pantano & Sarkar (2002), but the spatial resolution is twice as fine to properly represent the dissipative range of wave numbers.

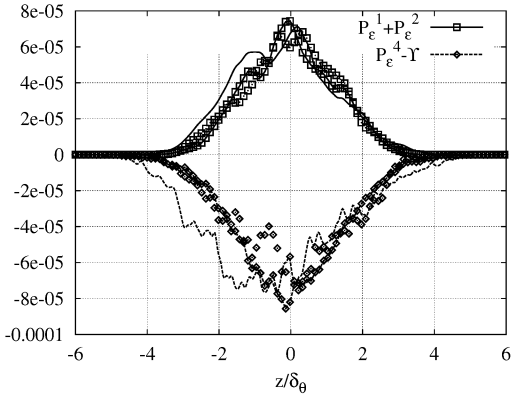

Figure 6: Production and destruction terms in the ε-equation; M10 (symbols), M11 (lines & symbols) and M14 (lines)

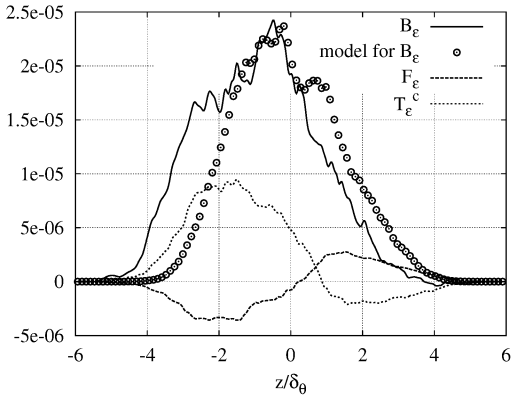

Figure 7: Explicit compressibility terms in the ε-equation; M14

The mean velocity profiles are independent of Mach number. A density difference between the two streams causes the center of the mixing layer, identified by the peak in K, to be shifted by one momentum thickness into the low density region as a result of mean momentum conservation and all profiles to become asymmetric. In order to compare the flows, data from M14 is always plotted over the shifted coordinate $z/\delta_\theta + 1$.

In the balance of the dissipation rate, P_ε^1 and P_ε^2 are not affected by either Mach number or density difference. However, P_ε^4 and $-\Upsilon$ vary under the different conditions, but their sum does not change substantially (see Fig. 6). The turbulent transport T_ε was found to decrease with Mach number; however, the density difference causes it to rise at the low density side, reflecting the shift of the mixing layer (see Fig. 10).

The compressible terms T_ε^c and F_ε have positive nonzero values at the center in the case with high Mach number (M11),

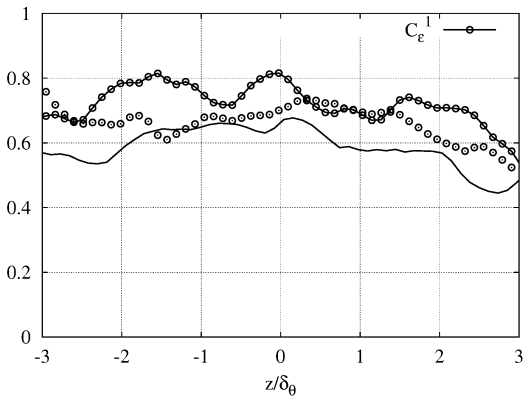

Figure 8: C_ε^1; M10 (symbols), M11 (lines & symbols) and M14 (lines)

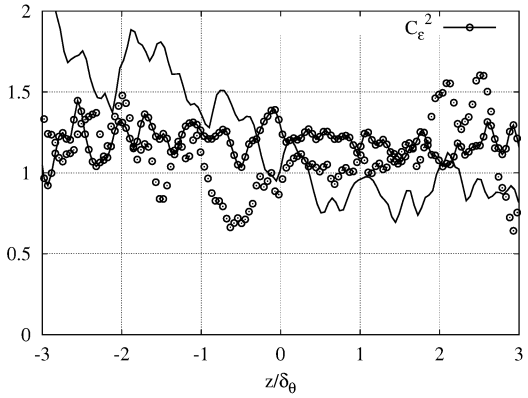

Figure 9: C_ε^2; M10 (symbols), M11 (lines & symbols) and M14 (lines)

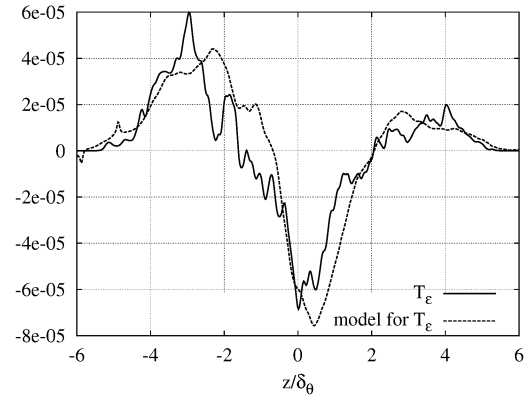

Figure 10: T_ε and its model, $f_t = 0.5$; M14

but they remain small compared to the other terms. The value of the baroclinic term B_ε is even smaller.

However, in the mixing layer case with a density difference (M14), B_ε becomes as big as P_ε^1 and has a similar shape. The compressible transport acts to redistribute the effects of dissipation from the high to the low density side. The term F_ε is somewhat smaller and has an opposite effect (Fig. 7). B_ε has to be modeled (see below), while the summed contribution of F_ε and T_ε^c still can be neglected.

The *a priori* tests using the mixing layer data can only give reasonable values for model coefficients in the inner part of the mixing layer, because at the edges both the exact terms and

the modeled terms are much too small for meaningful comparisons. In the inner part of the mixing layer ($-3 < z^* < 3$), Fig.8 shows that C_ε^1 is nearly independent of compressibility effects. There, the mean values and standard deviations are 0.66 ± 0.05, 0.72 ± 0.06 and 0.59 ± 0.06 for M10, M11 and M14. The value of C_ε^2 shows more irregularity, but the mean values of 1.11 ± 0.22, 1.20 ± 0.09 and 1.23 ± 0.39 for M10, M11 and M14 are close together.

Once again, the model for the turbulent transport term and the associated model coefficient are difficult to evaluate since T_ε changes sign within the layer. It is more instructive to compare model and exact term directly. (Due to oscillations resulting from the evaluation of the terms in the model, a box filter with filter-width δ_θ was used to smooth the profiles.) For all flow cases the agreement between model and exact term is good, if $f_t = 0.5$. For example, the M14 case in Fig. 10 shows very good agreement across the layer.

Since the terms P_ε^3 and D_ε are negligible in the mixing layer, models for these terms are not tested.

MODELING OF THE BAROCLINIC TERM

The model for B_ε should fulfill the following conditions: (i) it should act as a source in the equation – it is only negative in situations where it is negligible; (ii) since it is only relevant in situations with mean density gradients, the model should include this factor; (iii) it should either scale as the other terms in the dissipation rate balance or vanish for infinite Reynolds number – otherwise no self-similar solution is possible. The model assumptions are checked using data from the mixing layer case M14.

At the outset, it has to be determined which correlation appearing in the term $B_\varepsilon = 2\bar{\nu}\overline{(u'_{i,j} - u'_{j,i})\rho_{,j}p_{,i}/\rho^2} = -2\bar{\nu}\,\overline{\vec{\omega}' \circ (\nabla p \times \nabla\rho)/\rho^2}$ has to be modeled. A first step is to separate the division by the squared density from the term:

$$\begin{aligned}\overline{\vec{\omega}' \circ (\nabla p \times \nabla\rho)/\rho^2} &= \overline{\vec{\omega}' \circ (\nabla p \times \nabla\rho)}/\bar{\rho}^2 \\ &+ \sum_{n=1}^{\infty} \overline{\vec{\omega}' \circ (\nabla p \times \nabla\rho) \cdot \left(-2\frac{\rho'}{\bar{\rho}} - \frac{\rho'^2}{\bar{\rho}^2}\right)^n} \quad (8)\end{aligned}$$

It can be shown from the DNS data, that the correlations with density fluctuations do not contribute substantially to the term.

Following Krishnamurty & Shyy (1997), the correlation in the first term on the RHS of Eq.(8) can be split into

$$\begin{aligned}\overline{\vec{\omega}' \circ (\nabla p \times \nabla\rho)} &= \underbrace{\overline{\vec{\omega}' \circ (\nabla p' \times \nabla\bar{\rho})}}_{Term1} \\ &+ \underbrace{\overline{\vec{\omega}' \circ (\nabla\bar{p} \times \nabla\rho')}}_{Term2} + \underbrace{\overline{\vec{\omega}' \circ (\nabla p' \times \nabla\rho')}}_{Term3} \quad . (9)\end{aligned}$$

They concluded from an order of magnitude analysis, that the second term is the dominant one. However, the present DNS data leads to another conclusion, namely that the triple correlation ($Term3$) dominates. It is not possible then to simplify and model only the second-order terms.

The modeling approach is to represent the scalar and vector products by rms-values and a correlation coefficient:

$$\begin{aligned}\overline{\vec{\omega}' \circ (\nabla p \times \nabla\rho)} &= \overline{\vec{\omega}' \circ (\nabla p \times \nabla\rho)'} \\ &\approx C \cdot \omega'_{rms} \cdot (\nabla p \times \nabla\rho)'_{rms} \ , \quad (10)\end{aligned}$$

$$(\nabla p \times \nabla\rho)'_{rms} \approx C_{p\rho} \cdot \nabla p'_{rms} \cdot \nabla\rho'_{rms} \ . \quad (11)$$

In this approach only $\omega'_{rms} = \sqrt{\varepsilon/\bar{\nu}}$ is closed. $\nabla p'_{rms}$, $\nabla\rho'_{rms}$ and the coefficients C and $C_{p\rho}$ have to be modeled.

It is assumed that the hydrodynamic pressure fluctuations $p'_{rms} \sim \bar{\rho}q^2$ are the relevant ones [1] . Acoustic fluctuations are assumed not to contribute to the baroclinic term, since in a sound wave density gradients are parallel to pressure gradients. To get an estimate for the gradient, the relevant length scale has to be chosen. Using the assumption of an inertial range, Batchelor (1951) estimated the fluctuating pressure gradient as $1.17 Re_l^{\frac{1}{4}} \rho q^2/l = 1.17\rho q^2/\sqrt{l\lambda}$. In a later work, George *et al.* (1984) divided the fluctuating pressure gradient into a mean field–turbulence interaction part that dominates in the case of small Reynolds number, and a turbulence–turbulence interaction part. The first was modeled as $1.46 S^* \rho q^2/l$, and the second as $\sqrt{1.30 Re_l^{1/2} - 50.83}\,\rho q^2/l$. For infinite Reynolds number, the model becomes $1.14 Re_l^{\frac{1}{4}} \rho q^2/l$, which is similar to Batchelor's estimate. According to these theoretical findings the model for $\nabla p'_{rms}$ has the form

$$\nabla p'_{rms} \approx C_p \cdot \frac{\rho q^2}{\sqrt{\lambda l}} = C_p \cdot \frac{\rho\varepsilon^{3/4}}{\bar{\nu}^{1/4}} \ . \quad (12)$$

The density fluctuations are estimated by a mixing length model. Since the mixing is affected by both the large and small scale structures, an intermediate length scale between the integral scale and the Taylor microscale would be appropriate. As the length scale for the gradient, the Taylor microscale is chosen, similar to velocity gradients.

$$\nabla\rho'_{rms} \approx C_\rho \cdot \frac{|\nabla\bar{\rho}|\sqrt{\lambda l}}{\lambda} = C_\rho \cdot |\nabla\bar{\rho}| \cdot (\frac{q^4}{\bar{\nu}\varepsilon})^{1/4} \quad (13)$$

Combining the results from Eqs. (10) to (13) yields the model

$$B_\varepsilon \approx 2\,C_{B_\varepsilon} \left(\frac{|\nabla\bar{\rho}|}{\bar{\rho}}\right) q\varepsilon \quad (14)$$

It can immediately be seen that B_ε is proportional to the mean density gradient as required by condition (ii). Since in the mixing layer $\varepsilon \sim \Delta U^3/\delta_\theta$, $q \sim \Delta U$ and $\nabla\bar{\rho} \sim \bar{\rho}/\delta_\theta$, the complete model scales like $\Delta U^4/\delta_\theta^2$. This is the same scaling as the models for production, destruction and turbulent transport, so condition (iii) is fulfilled. It remains to determine the sign of the closure coefficient C_{B_ε} to insure condition (i) is met.

The assumptions associated with Eqs. (10) to (13) can be validated, and the model coefficients calibrated for the mixing layer M14 data. The *a priori* evaluation of the model given in Eq. (10) between ω' and $(\nabla p \times \nabla\rho)'$ yields a value for C. Figure 11 shows the distribution across the layer. Its mean value for $-3 < z^* < 3$ is -0.07. Additionally, Eqs. (12) and (13) yield values for C_p and C_ρ of 3.1 and 1.2, respectively. The value for C_p is roughly 2.5 times higher than the value predicted by Batchelor (1951) for high Reynolds number isotropic turbulence.

Writing the vector product in Eq. (11) in terms of the magnitude of the vectors and the angle ϕ between them gives

$$(\nabla p \times \nabla\rho)'^2_{rms} = \overline{(|\nabla p'||\nabla\rho'|sin\phi)^2} \approx C_{p\rho}^2\,\overline{|\nabla p'|^2}\,\overline{|\nabla\rho'|^2} \ . \quad (15)$$

[1] Here $Re_l = \frac{ql}{\nu}$, $Re_\lambda = \frac{q\lambda}{\nu}$, $l = \frac{q^3}{\varepsilon}$, $\lambda = \sqrt{\frac{\nu q^2}{\varepsilon}}$, $q = \sqrt{2K}$ and $S^* = \frac{SK}{\varepsilon}$ are used, where S is the mean velocity gradient.

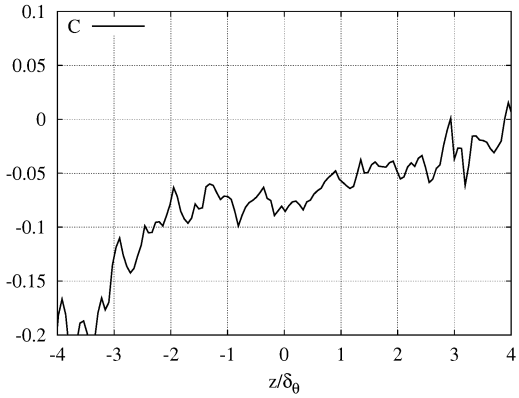

Figure 11: Model constant C (eq. (10))

If it is assumed, that both the direction and magnitude of the gradients of pressure and density are uncorrelated, the above equation simplifies to

$$\overline{sin^2\phi} \approx C_{p\rho}^2 \,. \tag{16}$$

The pdf $f(\psi)$ of ϕ needed to determine the value of $C_{p\rho}$ is $\frac{1}{2}sin\psi$ under these assumptions [2]. So

$$C_{p\rho} = \sqrt{\int_0^\pi 1/2 \cdot sin(\psi) sin^2(\psi) d\psi} \approx 0.816 \,. \tag{17}$$

This value slightly over-predicts the term in the mixing layer, but is close to the value of 0.7 determined from an *a priori* evaluation of the term. The assumption of independence of the gradients is not perfect, but does give a good estimate.

The comparison between the exact term B_ε and its model using $C_{B_\varepsilon} = 0.18$ ($\approx 0.07 \cdot 0.7 \cdot 3.1 \cdot 1.2$) shows, that the model works well (see Fig. 7). Only the shift of the term into the low density region, in addition to the shift of the whole layer, is not correctly predicted since C is taken as constant (although it is rising towards the low density region, Fig. 11).

SUMMARY

An examination of terms in the solenoidal dissipation rate equation (1) shows added contributions from explicit compressibility terms in addition to terms that also appear in incompressible flows. A new partitioning of these terms facilitates the identification of compressibility effects in the development of closure models for the new explicit compressibility terms as well as the standard terms appearing in both the incompressible and compressible formulations. The *a priori* analysis using DNS databases presented here leads to the following conclusions:

(i) Near cooled walls strong mean property variations are induced. The terms in the transport equation of solenoidal dissipation rate are in most cases reduced by compressibility.

(ii) The tests show that the coefficients in the modeled terms of the solenoidal dissipation rate equation are independent of Mach number and mean property variation. It can be concluded that the compressibility effects in the transport equation for ε are of indirect nature. This is reasonable, because compressibility effects should be proportional to the turbulent Mach number $M_t = u/c$ and the gradient Mach number $M_g = Sl/c$. Both parameters are related to large structures, and the small structures relevant for dissipation, scale with the Kolmogorov scales. Both the Kolmogorov length scale η and velocity scale u_η are very small, so the corresponding Mach numbers are close to zero and no direct compressibility effects are expected. Provided good incompressible models are available for all terms, their adapted forms will also be good models for compressible computations.

(iii) The argument of the relevant Mach numbers used above can also explain why the explicit compressibility terms are negligibly small in most cases. In the only flow where these terms are of non-negligible size, the mixing layer with high mean property variation, this is not caused by high Mach number, but by low Mach number mixing of fluid of different density. For the baroclinic term B_ε a model is proposed. The other two terms, F_ε and T_ε^c, are not modeled, because their combined contribution can be neglected.

Even though these results are relevant to a wide variety of flows, the conclusions are not universal. They have been obtained for compressible flows without shocks and without relevant changes of density or viscosity along a mean flow streamline. In flows where these phenomena appear, additional effects may arise.

REFERENCES

G. K. Batchelor. Pressure fluctuations in isotropic turbulence. *Proc. Camb. Phil. Soc.*, 47:359–374, 1951.

H. Foysi, S. Sarkar, and R. Friedrich. Compressibility effects and turbulence scalings in supersonic channel flow. *J. Fluid Mech.*, 509:207–216, 2004.

W. K. George, P. D. Beuther, and R. E. A. Arndt. Pressure spectra in turbulent free shear flows. *J. Fluid Mech.*, 148:155–191, 1984.

K. Hanjalić and B.E. Launder. A Reynolds stress model of turbulence and its application to thin shear flows. *J. Fluid Mech.*, 52:609–638, 1972.

V.S. Krishnamurty and W. Shyy. Study of compressibility modifications to the $k-\varepsilon$ turbulence model. *Phys. Fluids*, 9(9):2769–2788, 1997.

C. Pantano and S. Sarkar. A study of compressibility effects in the high-speed turbulent shear layer using direct simulation. *J. Fluid Mech.*, 451:329–271, 2002.

W. Rodi and N.N. Mansour. Low Reynolds number $k-\epsilon$ modeling with the aid of direct simulation data. *J. Fluid Mech.*, 250:509–529, 1993.

K. Sinha and G. V. Candler. Turbulent dissipation-rate equation for compressible flows. *AIAA Journal*, 41(6):1017–1021, June 2003.

[2] Only the directions of the gradients, two independent unit vectors, are considered. If the first vector is regarded as one axis of a sphere of radius $R = 1$, the second vector points from the center of the sphere to a point on its surface, and on each point with the same probability. Now the probability of $\phi < \psi$ equals the ratio between the segment of the surface of the sphere with $\phi < \psi$ and the whole surface of the sphere

$$F(\psi) = P\{\phi < \psi\} = \frac{\pi 2R^2(1 - cos(\psi))}{4\pi R^2} = \frac{1}{2}(1 - cos(\psi))$$

So the probability density function is

$$f(\psi) = \frac{dF(\psi)}{d\psi} = \frac{1}{2}sin(\psi).$$